Post-print of: Rivas Ubach, A. et al. "Coping with iron limitation: a metabolomic study of Synechocystis sp. PCC 3803" in Acta physiologiae plantarum (Ed. Springer), vol. 40, art. 28 (Feb. 2018). The final versión is available at DOI 10.1007/s11738-018-2603-1

# Coping with Iron Limitation: A Metabolomic Study of *Synechocystis sp*. PCC 6803.

Albert Rivas-Ubach[1,2†*], Amisha T. Poret-Peterson[3†], Josep Peñuelas[2,4], Jordi Sardans[2,4], Míriam Pérez-Trujillo[5], Cristina Legido-Quigley[6], Michal Oravec[7], Otmar Urban[7], James J. Elser[8]

1. Environmental Molecular Sciences Laboratory, Pacific Northwest National Laboratory, Richland, WA, USA, 99354
2. CREAF, Cerdanyola del Vallès, 08913 Catalonia, Spain
3. School of Earth & Space Exploration, Arizona State University, Tempe, Arizona 85287, United States
4. CSIC, Global Ecology Unit CREAF-CEAB-CSIC-UAB, Cerdanyola del Vallès, 08913 Catalonia, Spain
5. Service of Nuclear Magnetic Resonance, Faculty of Sciences and Biosciences, Universitat Autònoma de Barcelona, Bellaterra 08193, Barcelona, Catalonia, Spain
6. King's College London, Institute of Pharmaceutical Science, London SE1 9NH, England
7. Global Change Research Institute, Czech Academy of Sciences, Bělidla 986/4a, CZ-603 00 Brno, Czech Republic
8. School of Life Sciences, Arizona State University, Tempe, AZ 85287-4501, USA

† Authors contributed equally to the manuscript.
*Corresponding author.

**E-mail addresses:**
Albert Rivas-Ubach: albert.rivas.ubach@gmail.com
Amisha T. Poret-Peterson: aporetpe@asu.edu
Josep Peñuelas: josep.penuelas@uab.cat
Jordi Sardans: j.sardans@creaf.uab.cat
Míriam Pérez-Trujillo: miriam.perez@uab.cat
Cristina Legido-Quigley: cristina.legido_quigley@kcl.ac.uk
Michal Oravec: oravec.m@czechglobe.cz
Otmar Urban: urban.o@czechglobe.cz
James J. Elser: j.elser@asu.edu

**Corresponding author:**
Albert Rivas-Ubach
Environmental Molecular Sciences Laboratory,
Pacific Northwest National Laboratory,
3335 Innovation Boulevard, Richland, WA 99354, USA

Recent institution for Amisha T. Poret-Peterson:
USDA-ARS, Crops Pathology and Genetics Research Unit,
University of California, Davis, CA 95616, USA

**Abstract**

Iron (Fe) is a key element for all living systems, especially for photosynthetic organisms because of its important role in the photosynthetic electron transport chain. Fe limitation in cyanobacteria leads to several physiological and morphological changes. However, the overall metabolic responses to Fe limitation are still poorly understood. In this study, we integrated elemental, stoichiometric, macromolecular, and metabolomic data to shed light on the responses of *Synechocystis sp*. PCC 6803, a non-$N_2$-fixing freshwater cyanobacterium, to Fe limitation. Compared to *Synechocystis* growing at nutrient replete conditions, Fe-limited cultures had lower growth rates and amounts of chlorophyll *a*, RNA, RNA:DNA, C, N, and P and higher ratios of Protein:RNA, C:N, C:P and N:P, in accordance with the growth rate hypothesis which predicts faster growing organisms will have decreased biomass RNA contents and C:P and N:P ratios. Fe-limited *Synechocystis* had lower amounts Fe, Mn and Mo, and higher amount of Cu. Several changes in amino acids of cultures growing under Fe limitation suggest nitrogen limitation. Additionally, we found substantial increases in stress-related metabolites in Fe-limited cyanobacteria such antioxidants. This study represents an advance in understanding the stoichiometric, macromolecular and metabolic strategies that cyanobacteria use to cope with Fe limitation. This information, moreover, may further understanding of changes in cyanobacterial functions under scenarios of Fe limitation in aquatic ecosystems.

**Key words: metabolomics, metallomics, iron limitation, cyanobacteria, ecological stoichiometry**

## Introduction

Metabolomics aims to characterize the metabolome of organisms and it is gaining importance in fields such as microbiology, plant physiology, and more recently in ecology (Macel et al. 2010; Jones et al. 2013; Rivas-Ubach et al. 2014; 2016a). The metabolome consists of all the low molecular weight compounds (metabolites) present in an organism at a given time (Fiehn 2002) constituting all of the compounds involved in physiological processes allowing cells to function, grow, and respond to environmental stressors (Peñuelas and Sardans 2009). The metabolome can be considered, thus, as the “chemical phenotype” of an organism (Fiehn 2002).

Any fine-scale shifts in metabolites may underpin higher-order shifts in cellular macromolecular composition (e.g. changes in overall protein and nucleic acid composition) and stoichiometry (Rivas-Ubach et al. 2012) and can thus, in turn affect the whole-organism requirement for key nutrient elements such as C, N, and P, forming the basis of what is now known as "biological stoichiometry" (Sterner and Elser 2002; Elser et al. 2008). Furthermore, environment-induced metabolic shifts can also affect the profile of less-abundant elements, such as the suite of essential metals that make up an organism's metallome (Silva and Williams 2001). Indeed, emerging studies have shown how metabolomes can be related to biomass stoichiometry and growth rate. For example, Rivas-Ubach et al. (2012) found that changes in foliar C:N:P:K stoichiometry of the Mediterranean shrub *Erica multiflora* were related to shifts in the metabolome of leaves during growing seasons and across soil moisture regimes. Such relationships between metabolomes, biomass stoichiometry, and growth rate may also occur in other organisms. In this study, we integrated metabolomics, macromolecular and stoichiometric analyses of a model freshwater unicellular cyanobacterium, *Synechocystis sp.* PCC 6803, grown under iron (Fe) limited conditions.

Fe is required for many enzymes necessary for physiological processes, such as respiration (Richardson 2000), nitrogen reduction and assimilation (Bellenger et al. 2011), and

especially photosynthesis (Ferreira and Straus 1994; Raven et al. 1999; Behrenfeld 1999; Shcolnick and Keren 2006). In cyanobacteria, photosystem I (PS I) and photosystem II (PS II) complexes of the photosynthetic electron transport chain (PETC) are Fe-rich with 12 and 3 Fe atoms, respectively (Ferreira and Straus 1994), and 6 Fe atoms in the cytochrome b6/f complex (Baniulis et al., 2008). This results in a high cellular Fe quota with ~4 x $10^6$ Fe atoms per cell for *Synechocystis sp*. PCC 6803 (Keren et al. 2004). The high content of Fe in the PETC and its low availability make this element a key limiting nutrient for photoautotrophs in many ecosystems (Behrenfeld et al. 1996; 1999; Vrede and Tranvik 2006; Mackey et al. 2015). Additionally, Fe bioavailability is further influenced by physico-chemical properties of water such as acidity which is expected to increase in many aquatic ecosystems in the forthcoming decades (Shi et al. 2010; Shi et al. 2012).

Cyanobacteria exhibit several morphological and physiological responses to Fe deficiency including the release of intracellular Fe from storage complexes (Keren et al. 2004; Shcolnick et al. 2009), induction of high-affinity Fe uptake systems (Katoh et al. 2001a; Katoh et al. 2001b; Kranzler et al. 2014), and decreases in photosynthetic capacity, phycobilisomes, chlorophyll and other pigments, cell yields, and growth rates (Ferreira and Straus 1994; Dang et al. 2012). Alterations in gene and protein expression underlie most of the morphological and physiological responses of cyanobacteria to Fe limitation (Castielli et al. 2009; Hernández-Prieto et al. 2012; Kopf et al. 2014).

Metabolomic changes in cyanobacteria and especially in *Synechocystis sp.* PCC 6803, under low Fe availability are not well-documented. Since metabolomes are the final product of genomes (Fiehn 2002), we expect that transcriptomic and proteomic changes of cyanobacteria in response to Fe deprivation should be reflected in their metabolomes. More specifically, the reduced photosynthetic capacity of Fe-limited cyanobacteria should trigger changes in C and N metabolism that are detectable as differences in the abundance of metabolites. We used metabolomics approaches in combination with macromolecular and elemental analyses to

characterize the metabolomes and the C, N, P, trace metal, DNA, RNA, and protein contents to obtain a better overall understanding of the effects of Fe limitation on the physiological status of wild type *Synechocystis sp.* PCC 6803. Data obtained are interpreted with the aim of integrating metabolomics with biological stoichiometry to provide important information for understanding the impacts of Fe limitation on communities and on biogeochemical cycling in marine and freshwater ecosystems.

## Materials & Methods

### *Growth of Synechocystis sp. PCC 6803*

*Synechocystis sp.* PCC 6803 (hereafter *Synechocystis*) was grown in 1.8 L of BG-11 medium pH 7.8 (Allen 1968) in 2 L trace metal clean polycarbonate bottles at 24 °C under continuous aeration with 0.2 μm filtered air and illumination (50 μmol photons $m^{-2}$ $s^{-1}$ irradiance). During the exponential phase of growth, cells were harvested and transferred to normal composition BG-11 (N:P 100, 18 μM Fe) or modified BG-11 to assess the effect of Fe limitation (N:P 100, 1.8 μM Fe) on physiological processes in *Synechocystis*. Six replicates were grown for *Synechocystis* cultures growing at complete media conditions and for the cultures growing at Fe-limited conditions. Upon transfer of *Synechocystis* to each bottle, the growth rate of the cultures was monitored via absorbance at 730 nm and once cultures reached exponential growth (7 days for complete, and 10 days for Fe-limited cultures), cells were harvested for the following analyses: (1) absorbance and chlorophyll *a*, (2) cell counts, (3) elemental composition (C, N, P, S, and trace metals), (4) biological macromolecule composition (DNA, RNA, and protein), and (5) metabolomic profiling. Three cultures from each treatment were also selected for transcriptomic analyses in a separate study (Kellom et al., unpublished).

### *Growth rate, absorbance spectra, and chlorophyll a measurements*

The growth rate and final yield of *Synechocystis* for each treatment was assessed via

absorbance at 730 nm and chlorophyll *a* measurements, respectively. Absorbance spectra from 350 to 800 nm on 0.5 mL of culture were also obtained using a Beckman Coulter DU®730 UV/Vis Spectrophotometer (Beckman Coulter, Indianapolis, IN, USA). The growth rate (GR) of cultures was calculated as follows:

$$GR[d^{-1}] = \frac{\ln\left(\frac{Abs_{730nm}(time\ n)}{Abs_{730nm}(time\ 0)}\right)}{\Delta\ time\ (days)}$$

Chlorophyll *a* was measured on 2 mL of culture harvested via centrifugation at 21,000 × *g* for 10 minutes at 4°C. Supernatant of all tubes was removed and cell pellets were extracted with 1 mL of 100% methanol for 5 minutes in the dark at room temperature (24 °C). After centrifugation (21,000 × *g*; 5 min; 4 °C) to collect cell debris, the supernatant was transferred into a polystyrene cuvette to measure the absorbance of cell extracts at 665 nm. Methanol (100%) was used as blank. Chlorophyll *a* ($Chl_a$) concentration (µg $mL^{-1}$) was calculated as follows (Bennette et al. 2011):

$$Chl_a[ug \cdot mL^{-1}] = 13.9 \cdot Abs_{665nm}$$

*Cell imaging and cell count measurements*

*Synechocystis* cells were imaged via epifluorescence microscopy to check for contamination and final cell counts were performed using an automated particle counter. Epifluorescence microscopy was performed on 10 µL culture aliquots fixed with 4% formaldehyde, deposited onto PTFE-coated microscope slides, and DAPI stained. Cells were imaged at 1000X magnification. Cell counts were conducted using the Multisizer™ 3 Coulter Counter (Beckman Coulter, Indianapolis, IN, USA) equipped with a 20 µm aperture tube (0.4 to 12.0 µm dynamic range for determination of particle size) on 50 to 1000-fold dilutions of culture.

After transcriptomic analysis, we found 16S rRNA gene sequences from *Hymenobacter*, a rod-shaped bacterium ranging in length from 2 to 6 µm (Krieg et al. 2010). Visual inspection of cultures via epifluorescence microscopy revealed the presence of a few rod-shaped cells

(approximately 2-4 μm in length) in some fields. However, all cultures displayed a single particle size peak of approximately 1.63 ± 0.08 μm using the Coulter counter suggesting minor contamination by this rod-shaped bacterium.

*Elemental composition measurements*

The concentrations of C, N, P, and trace metals (Ca, Co, Cu, Fe, Mg, Mn, Mo, Ni, Zn, and V) in *Synechocystis* were measured following incubation. For C and N analyses, 30 mL of cells from each culture bottle were harvested and centrifuged at 5,000 × *g* for 10 minutes at 4°C and washed with 0.85% NaCl to remove excess media. Samples (200 mL) for P, S, and trace metal analyses were equally harvested and washed three times with an oxalic acid solution (pH 7.8, 50 mM $Na_2EDTA$, 100 mM oxalic acid, 304 μM $MgSO_4 \cdot 7H_2O$, 245 μM $CaCl_2 \cdot 2H_2O$, and 189 μM $Na_2CO_3$) to remove extracellular Fe and other metals (Tovar-Sanchez et al. 2003). Cell pellets were stored at -80°C until analyses.

For C, N, P, and trace metal determination, samples were dried for 24 hours at 60°C. C and N were measured on 1-3 mg dry weight samples using a Costech Elemental Analyzer coupled to a Finnigan DeltaPlus Isotope Ratio Mass Spectrometer (EA-IRMS; Thermo-Finnigan MAT 253, West Palm Beach, FL, USA). C and N contents were calculated via comparison with a tomato leaves standard (NIST SRM 1573a).

P, S, and trace metals were measured on 50 to 120 mg dry weight of samples digested three times overnight at 100°C with 5 mL of 16 M nitric acid. After digestion, samples were dried and resuspended in 5 mL of 0.32 M nitric acid. Samples were diluted 15- and 100-fold to measure the following elements: Ca, Co, Cu, Fe, Mg, Mn, Mo, Ni, P, S, V, and Zn. Calibration curves were constructed for the elements using a phosphorus-enriched black-shale standard of known elemental composition. Trace metals were measured via Inductively-Coupled Plasma Mass Spectrometry (ICP-MS; iCAP Q ICP-MS, Thermo Fisher Scientific, Waltham, MA, USA). EA-

IRMS and ICP-MS measurements were carried out in the W. M. Keck Foundation Laboratory for Environmental Biogeochemistry at Arizona State University.

*Biological macromolecule (DNA, RNA, and protein) composition analyses*

DNA was extracted from 20 mL of cells using the FastDNA® Spin Kit and FastPrep®-24 homogenizer (MP Biomedicals, Solon, OH, USA) following the manufacturer's protocol. DNA was quantified via fluorescence using the PicoGreen assay kit (Invitrogen, Carlsbad, CA, USA).

RNA was extracted from 20 mL of cells using the FastRNA® Pro Blue Kit (MP Biomedicals, Solon, OH, USA) following the manufacturer's protocol with the following exception. A second chloroform extraction was performed to further purify nucleic acids and samples were precipitated overnight with isopropanol at -20°C. To remove gDNA, samples were treated with the RTS DNase (MO BIO Laboratories, Carlsbad, CA, USA) according to the manufacturer's protocol. DNased RNA was purified via the RNeasy MinElute Cleanup Kit (Qiagen, Valencia, CA, USA) and RNA concentration was measured using the Qubit® RNA Assay Kit (Invitrogen, Carlsbad, CA, USA) following the manufacturer's instructions.

Protein was extracted from 20 mL of cells using a protocol modified from Gao et al. (2009). Briefly, cells were resuspended in 500 µL of 10 mM HEPES-NaOH (pH 7.2) amended with 1X Protease Inhibitor Cocktail (Promega, Madison, WI, USA). Resuspended cells were transferred to Lysing Matrix B tubes (MP Biomedicals, Solon, OH, USA) and homogenized for 45 s at a speed of 6.0 m $s^{-1}$ in a FastPrep®-24 homogenizer. Samples were centrifuged at 5,000 × *g* for 5 minutes at 4°C to pellet cellular debris and lysing beads. 250-300 µL of supernatant was transferred to another tube and the protein concentration measured using the Qubit® Protein Assay Kit (Invitrogen, Carlsbad, CA, USA) following the manufacturer's instructions.

*Metabolite extraction*

The remaining biomass (from ~800 mL of culture) was reserved for metabolomic analyses. Cell pellets were rapidly frozen in liquid nitrogen and lyophilized (Rivas-Ubach et al. 2013). Lyophilized cells were stored at -80 °C until metabolite extraction.

***Metabolite extraction for NMR analyses:*** Polar and semi-polar metabolites were extracted by following Rivas-Ubach *et al.* (2013). Briefly, 30 mg of lyophilized cells from each sample was extracted in 6 mL of water/methanol (1:1) via vortexing and sonication. These procedures were repeated for two extractions of the same sample. Sample extracts where lyophilized and 1 mL of $KH_2PO_4$-buffered $D_2O$ + 0.01% TSP (trimethylsilyl propionic acid sodium salt) (pH 6.0) was added. TSP was used as internal standard. Extracts were transferred to NMR sample tubes and analyzed as detailed in Rivas-Ubach *et al.* (2013).

***Metabolite extraction for LC-MS analyses:*** Metabolites were extracted following t'Kindt *et al.* (2008) with minor modifications. Two sets of 2 mL centrifuge tubes tubes were labeled: set A for extractions of samples and set B for keeping the extracts from set A. 30 mg of lyophilized cells of each sample was transferred to set A tubes and 1 mL of methanol/water (80:20) was added to each tube. Set A was vortexed for 15 min, sonicated for 5 min at room temperature and centrifuged at 23,000 × *g* for 5 min. After centrifugation, 0.6 mL of the supernatant from each tube was transferred to the corresponding set B tubes. This procedure was repeated again for two extractions of the same sample and the second aliquot was combined with the previous one. The set B tubes were then centrifuged at 23,000 × *g* for 5 min. The supernatants were collected by crystal syringes, filtered through 0.22 µm pore microfilters and transferred to a labeled set of HPLC vials. The vials were stored at -80 °C until LC-MS analysis.

*Metabolomic measurements of cellular extracts*

***NMR-based metabolomics:*** NMR experiments were performed on a Bruker AVANCE 600 spectrometer (Bruker Biospin, Rheinstetten, Germany) working at a magnetic field of 14.1 T ($^{1}$H and $^{13}$C NMR frequencies of 600.13 and 150.13 MHz respectively) and equipped with an automatic sample changer, a multinuclear triple resonance TBI probe and a temperature control unit . The temperature into the probe head was previously calibrated and maintained constant for all the experiments at 24.5 ºC; for this purpose an equilibration delay (2 min) is left once the tube is into the magnet and prior to the shimming process. All NMR sample handling, automation, acquisition and processing were controlled using TopSpin 3.1 software (Bruker Biospin, Rheinstetten, Germany). Spectra were referenced to the internal reference TSP ($^{1}$H and $^{13}$C at δ 0.00 ppm).

***$^{1}$H NMR fingerprinting*:** Extracts were analyzed through standard pulse-acquisition one-dimensional (1D) $^{1}$H-NMR experiments with suppression of the residual water resonance. Water resonance signal was presaturated at a power level of 55 dB, corresponding to an effective field of 30 Hz during a relaxation delay of 2s. Samples were analyzed as a set of 32 k data points, over a spectral width of 16 ppm, as the sum of 128 transients and with an acquisition time of 1.7 s. The experimental time was ~8 min per sample. Fourier transformation was applied to the resulting interferograms (free induction decay, FID) and the spectra obtained were phased and baseline corrected. All FIDs of polar samples were multiplied by an exponential apodization function equivalent to 0.2 Hz line broadening prior to the Fourier transform.

***NMR metabolite identification*:** Standard 2D NMR experiments ($^{1}$H-$^{1}$H correlated spectroscopy (COSY), $^{1}$H-$^{1}$H total correlation spectroscopy (TOCSY), $^{1}$H-$^{13}$C heteronuclear single quantum correlation (HSQC) and $^{1}$H-$^{13}$C heteronuclear multiple bond correlation (HMBC)) and 1D selective $^{1}$H TOCSY experiments were performed in representative extract samples for the

identification of the metabolites. Experiments were acquired with standard presaturation of the residual water peak during the relaxation delay using standard Bruker pulse sequences and routine conditions. All assigned metabolites were further confirmed by reported literature data (Rivas-Ubach et al. 2012). See Table S1 of supporting information for identified metabolites with NMR.

***LC-MS analysis:*** LC-MS chromatograms were obtained using a Dionex Ultimate 3000 HPLC system (Thermo Fisher Scientific/Dionex RSLC, Dionex, Waltham, MA, USA) coupled to an LTQ Orbitrap XL high-resolution mass spectrometer (Thermo Fisher Scientific, Waltham, MA, USA) equipped with an HESI II (heated electrospray ionization) source. A reversed-phase C18 Hypersil gold column (150 × 2.1 mm, 3-µm particle size; Thermo Scientific, Waltham, Massachusetts, USA) was used for chromatography at 30 °C. Mobile phases were filtered and degassed for 10 min in an ultrasonic bath prior to use and consisted of 0.1% acetic acid in water (A) and acetonitrile (B). Sample injection volume was set at 5 µL. At a flow rate of 0.3 mL per minute, the elution gradient began at 90% A/10% B and was held for 5 min, and then the elution changed linearly to 10% A/90% B during the next 15 min. The initial proportions (90% A/90% B) were thus lineraly recovered over the next 5 min, and the column was washed and stabilized for 5 min. The Orbitrap operated in FTMS (Fourier Transform Mass Spectrometry) full-scan mode with a mass range of 50-1000 m/z and high-mass resolution (60,000). The resolution and sensitivity of the spectrometer were monitored by injecting a standard of caffeine after every 10 samples, and the resolution was further monitored with lock masses (phthalates). All samples were injected twice, with the HESI operating in positive (+H) and (-H) ionization modes. Blank samples were also analyzed at the beginning of the sequence. See Rivas-Ubach *et al.* (2016b) for details of LC-MS methods.

*Metabolomic data processing*

***NMR bucketing*:** The processing of $^{1}$H NMR spectra is detailed in Rivas-Ubach *et al.* (2013). First, all $^{1}$H NMR spectra were phased, baseline corrected and referenced to the resonance of the internal standard (TSP) at δ 0.00 ppm with TOPSPIN 3.1. A variable-size bucketing was thus applied to all $^{1}$H NMR spectra with AMIX software (Bruker Biospin, Rheinstetten, Germany), scaling the buckets relative to the internal standard (TSP). The output was a data set containing the integral values of each $^{1}$H NMR peak in the described pattern. The buckets corresponding to the same molecular compound were summed.

***LC-MS chromatograms:*** The LC-MS RAW data files were processed by MZmine 2.17 (Pluskal et al. 2010). LC-MS chromatograms were baseline corrected and a list of ions was generated according to retention time and exact mass. Ion chromatograms were thus deconvoluted and posteriorly aligned, auto-assigned and numerical values of the area of the peaks were finally exported in CSV format (see Table S2 of supporting information for details). Metabolites were assigned by exact mass and retention time from the measurements of the standards in the spectrometer (see Table S3 of supporting information for details). Assignation of metabolites was based in two independent orthogonal data; exact mass of compounds and retention time (RT) relative to the standards. According to the Metabolomics Standards Initiative (Sumner et al. 2007), our LC-MS metabolomic results are thus based on putative identifications. However, the high mass accuracy of the Orbitrap technology (<10 ppm) and the use of RT reduce considerably the number of false positives (Rivas-Ubach et al., 2016b). As in NMR bucket tables, the different variables corresponding to the same molecular compounds were summed.

The area values obtained by the integration of the LC-MS chromatograms and and $^{1}$H-NMR spectra are directly related to the concentration of the corresponding variable even though they do not represent the real concentration in the sample. However, the use of those values are suitable for metabolomic comparative analyses as previously demonstrated in other

328 studies (Lee and Fiehn 2013; Mari et al. 2013; Leiss et al. 2013; Gargallo-Garriga et al. 2014;
329 2015; Rivas-Ubach et al. 2016c; 2017). In this study, we use the term *concentration* when
330 referring to changes in the relative amount of metabolites between the tested treatments.
331
332 *Statistical analyses*
333 The dataset for this study was analyzed as a function of the categorical independent variable
334 (treatment with two levels: complete and Fe-limited cultures) and 1451 dependent continuous
335 variables. Of these dependent variables, 24 were GR, cell density, elemental concentrations (C,
336 N, P, S, Fe, Ca, Mg, Mn, Zn, Cu, Ni, Co, Mo, and V), stoichiometric variables (C:N, C:P, and N:P),
337 macro-molecular variables (Protein, DNA, RNA) and macro-molecular ratios (RNA:DNA, and
338 Protein:RNA). The other 1427 were metabolomic variables, of which 34 were identified. First,
339 variables that were not normally distributed and/or lacked equal variances, assessed via the
340 Shapiro-Wilk and Levene's tests, respectively, were $\log_{10}$-transformed before statistical
341 inference.
342 To test for overall significant differences between metabolomes of the complete and Fe-
343 limited cultures, the metabolome fingerprints including the identified and the non-identified
344 metabolites (1427 variables), were subjected to PERMANOVA using the Euclidean distance
345 with treatment (complete and Fe-limited cultures) as ixed factor and permutations set at
346 10,000. Additionally, to understand how the metabolomic and physiological variables shifted
347 with Fe limitation, the whole data set (1451 variables) was subjected to principal component
348 analysis (PCA). For visualization purposes, only known metabolomic variables are represented
349 in the PCA (Figure 1). As expected, the first PC separated complete from Fe-limited cases and
350 only PC1 is shown in Figure 1. The score coordinates of the samples were subjected to t-test
351 to determine statistical significance in the case separation between treatments (Rivas-Ubach
352 et al. 2013).

T-tests were used to detect significant differences between treatments (complete versus Fe-limited) for each individual identified variable. The variables that did not meet the assumptions of t-tests after $\log_{10}$ transformation were compared using a Mann-Whitney U test.

All statistical analyses were performed with R (R Core Team 2013). The Shapiro-Wilk tests, t-tests and Mann-Whitney U tests were performed with the functions *shapiro.test*, *t.test*, and *wilcox.test* respectively from the package "stats" (R Core Team 2013). Levene's tests were performed with the *leveneTest* function in the "car" package (Fox and Weisberg 2011). The PERMANOVA analysis was conducted with *adonis* function in the package "vegan" (Oksanen et al. 2013). The PCA was performed by the *pca* function of the *mixOmics* package of R (Dejean et al. 2013).

**Results**

Growth of *Synechocystis* under Fe concentrations one-tenth of the normal composition of the BG-11 medium produced a blue shift in the chlorophyll absorbance peak from 679 to 673 nm (Figure S1), which is diagnostic of Fe-limitation in *Synechocystis* (Ryan-Keogh et al. 2012).

PCA including all the elemental, macromolecular, and metabolomic variables showed clear separation between complete and Fe-limited cultures along the first principal component (PC1), which gathered 28.4% of the total variance (Figure 1). This separation in the cases of each treatment along PC1 was statistically significant ($t = 10.98$; $P < 0.001$).

The growth rate, final cell density, and chlorophyll *a* content of cultures were significantly lower in Fe-limited than complete cultures (Figure 1; Table S4). Fe-limitation also resulted in significantly lower concentrations of C, N, P, S, Fe, Mg, Mn, Mo, RNA, and RNA:DNA ratios, and significantly higher Cu content, C:N, C:P, N:P and Protein:RNA ratios (Figure 1, Table S4).

The PERMANOVA indicated that the overall metabolomes of Fe-limited and complete *Synechocystis* varied significantly ($P < 0.01$) (Table 1). Several of the individual identified metabolites changed significantly between complete and Fe-limited cultures. Concentrations of $\alpha$-glucose, leucine, lysine, phenylalanine, proline, valine, lactic acid, malic acid, succinic acid and $\delta$-tocopherol increased significantly under Fe limitation ($P < 0.05$) (Figure 1; Table S5). Concentrations of disaccharides, hexoses, arginine and aspartic acid showed marginally significant ($P < 0.1$) increases in Fe-limited cultures (Figure 1; Table S5). AMP, glutamine and threonine decreased significantly ($P < 0.05$) and $\beta$-glucose decreased marginally significantly ($P < 0.1$) in Fe-limited cultures.

We found significant effects on the metallome (Ca, Cu, Co, Fe, Mg, Mn, Mo, Ni, Zn, and V) of *Synechocystis* grown under Fe-limited conditions (Table 2 and S4). Fe, Mg, Mn, and Mo contents and C:Fe, C:Mg, C:Mn, and C:Mo ratios decreased significantly under Fe limitation, while Cu content and C:Cu ratio increased significantly.

## Discussion

Lowering the Fe concentration to one-tenth of the normal composition of BG-11 resulted in Fe limitation of *Synechocystis*, as diagnosed by a characteristic blue shift in the chlorophyll absorbance peak (Figure S1; Wilson et al. 2007). This shift likely indicates the association of the chlorophyll-binding protein, iron stress-inducible protein (IsiA) with PSI to increase the size of the light-harvesting complex and possibly compensate for phycobilisome degradation (Bibby et al. 2001; Ryan-Keogh et al. 2012).

We found that our cultures contained cells of *Hymenobacter sp.* through transcriptomic sequencing (Kellom et al., unpublished) representing approximately 10% of the biomass across the cultures. However, this contamination should not be a major concern in our study. Organisms' metabolomes have proven to present large plasticity among biological replicates (Steuer et al. 2003; Houshyani et al. 2012; Rivas-Ubach et al. 2016a). Furthermore,

all the identified metabolites have been previously reported in *Synechocystis sp.* and our analyses are exclusively based on relative quantification and never in presence/absence. Therefore, the main differences between complete and Fe-limited are primarily due to the predominant *Synechocystis* biomass and any potential variation produced by *Hymenobacter sp*. would be masked in the overall metabolome variability. Additionally, the transcriptome of *Synechocystis* under Fe limitation was similar to previous studies (Kellom et al., unpublished) and was concordant with our observed results. Even so, we restricted our main conclusions to those bolstered by reference to previous studies.

*Fe limitation and the growth rate hypothesis*

The growth rate hypothesis (GRH) is one of the central paradigms in ecology and proposes that fast growing organisms increase the allocation of P to RNA to meet the high protein synthesis demand (Elser et al. 1996). Our stoichiometric and macromolecular results are in accordance with the GRH; Fe-limited *Synechocytis* showed slower growth than complete cultures and this was accompanied by decreases in RNA content and RNA:DNA ratio as well as the increases in C:P, N:P and Protein:RNA ratios (Figure 1, Table S4). The GRH has generally focused on conditions of N and/or P limitation or excess, however, our study suggests that other potential limiting factors such Fe can also induce lower growth rates through mechanisms involving changes in cellular N:P and Protein:RNA ratios.

*Indirect N starvation produced by limitation of Fe*

We observed potential links between metabolite abundances and biomass stoichiometry and note several metabolomic changes under Fe limitation suggesting a situation of N limitation. The lower C content in Fe-limited cultures (Figure 1; Table S4) strongly indicates a reduction in C fixation capacity under lower Fe availability (Sharon et al. 2014). Although no Calvin Cycle intermediates were identified in the metabolomes, Fe-limited

430 *Synechocystis* exhibited decreased gene expression of *rbcS*, encoding the small subunit of
431 ribulose-1,5-bisphosphate carboxylase/oxygenase (Kellom et al., unpublished). With reduced C
432 flux through the Calvin Cycle under Fe limitation, there may have been a decrease in the direct
433 precursor of purines, ribose-5-phosphate, resulting in the observed reduction in AMP and
434 other purine metabolites (Lengeler et al. 1999) (Figure 1) as observed in N-starved
435 *Synechocystis sp.* (Osanai et al. 2014).
436 We found significant changes in the abundances of some carbohydrates and
437 tricarboxylic acid cycle intermediates under Fe limitation (Figure 1; Table S5) that are similar to
438 responses to N limitation. It has been observed that *Synechocystis sp.* and other cyanobacteria
439 accumulate carbohydrates and precursors of glycogen (i.e., glucose and other hexoses
440 increased in Fe-limited cultures in this study) under N deprivation (Gründel et al. 2012;
441 Hasunuma et al. 2013; Osanai et al. 2014). Succinate is both a respiratory substrate and a C
442 substrate for biosynthesis. The decreased C content of Fe-limited along with higher
443 concentrations of succinate and malate (Figure 1; Table S5) suggest that succinate was
444 oxidized to malate via fumarate under limitation of Fe (Cooley and Vermaas 2001; Knoop et al.
445 2013). N starvation has proven to elicit a similar response in *Synechocystis sp.* with substantial
446 increases in succinate, malate, and fumarate (Osanai et al. 2014).
447 The significant reduction in N content and the increases in C:N ratio in Fe-limited
448 cultures indicate a state of N limitation, despite the high nitrate availability (17.6 mM). The
449 negative effect of Fe limitation on N uptake is feasible, as *Synechocystis sp.* and other
450 cyanobacteria down-regulate metabolites associated with N assimilation under C limitation
451 (Huege et al. 2011). The concentrations of many amino acids were significantly reduced in Fe-
452 limited cultures (Figure 1; Table S5) which also observed under N starvation (Osanai et al.
453 2014). Although Fe-limited stoichiometric and metabolomic responses suggest a status of N
454 limitation, macromolecular analyses indicated that protein synthesis did not decrease under Fe
455 limitation (Figure 1; Table S4). More focused research is necessary to better comprehend how

456 N is allocated to different physiological functions under Fe limitation and how this could
457 consequently impact the N cycle.
458
459 *Fe limitation and metabolites indicative of oxidative stress*
460 Oxygen radicals produced as a byproduct of photosynthesis and reduced Fe can
461 interact leading to oxidative stress through the Fenton Reaction (Latifi et al. 2009).
462 Transcriptomic studies in *Synechocystis sp.* have previously linked Fe and oxidative stress
463 (Singh et al. 2004; Shcolnick et al. 2009). Oxidative stress has also been described under Fe
464 limitation because of the redox imbalance between PS I and PS II and the reduced availability
465 of Fe as a cofactor for superoxide dismutase and catalase (Latifi et al. 2009). Fe-limited
466 cultures showed significant concentration increases of metabolites with antioxidant function
467 (δ-tocopherol, choline, and proline) (Figure 1; Table S5) suggesting a state of oxidative stress
468 under Fe limitation. Tocopherols concentration has already shown to be increased to cope
469 with lipid peroxidation in *Synechocystis sp.* (Maeda et al. 2005). We also found increases in
470 proline under Fe-limitation which has been described to increase in other cyanobacteria and
471 plants in response to oxidative stress induced by heavy metal toxicity and to cope with
472 increased salinity (Singh et al. 1996; Szabados and Savouré 2010). However, to the best of our
473 knowledge, increases in proline in *Synechocystis sp.* as response to oxidative stress produced
474 by Fe limitation has not been previously reported yet. Choline accumulation has been
475 described in salt acclimation responses of cyanobacteria (Hagemann 2011), however, choline is
476 also a precursor of glycine betaine which stabilizes proteins of the oxygen-evolving complex of
477 PS II (Papageorgiou and Murata 1995). Additionally, *Synechocystis sp.* is genetically competent
478 for D-lactate production via pyruvate reduction (D-lactate dehydrogenase encoded by *slr1556*)
479 (Kaneko et al. 1996) and we found increases in lactate concentrations in Fe-limited cultures
480 (Figure 1; Table S5). With decreased C uptake and potentially less consumption of NAD(P)H,
481 the NAD(P)H/NAD(P)$^+$ ratio of cells could be extremely imbalanced under Fe limitation. Our

metabolomic analyses suggest that the higher concentration of lactate in Fe-limited cultures could have been the consequence to consume excess NADH and regenerate $NAD^+$ as in fermentative metabolism (Lengeler et al. 1999). The production of antioxidants and lactate production would allow *Synechocystis sp.* to cope with a potential imbalanced NAD(P)H/$NAD(P)^+$ ratio indicating that responses to Fe limitation and redox homeostasis overlap in *Synechocystis sp*. Complementary analyses to our metabolomics measurements would be required to experimentally measure the cellular NAD(P)H/$NAD(P)^+$ to definitely verify and determine more precisely the redox status of cyanobacteria under Fe limitation.

*Flexibility in the metal composition of Synechocystis sp.*

Several trace metals have biologically important roles in photosynthetic and other metabolic processes, such as N assimilation. The differences in metal content between Fe-limited and complete cultures support a view that the metal composition of *Synechocystis sp.* is highly responsive to environmental conditions.

Low availability of Fe impacts the photosynthetic machinery of cyanobacteria through phycobilisome degradation, decreased chlorophyll content, and changes in the PETC (Ferreira and Straus 1994; Behrenfeld and Milligan 2013). Under Fe-limited conditions, cyanobacteria may partially reduce their need for this metal by replacement of Fe-containing redox proteins (cytochrome c553 and ferredoxin) with non-Fe dependent carriers (Cu-containing plastocyanin and FMN-containing flavodoxin, respectively) (Ferreira and Straus 1994). We observed that Fe-limited cultures in this study increased the expression of the genes encoding plastocyanin and flavodoxin (Kellom et al., unpublished). Our metallomic analyses showed significant decreases (approximately 3 times) in cellular Fe content and Fe:C ratio and increases in Cu content and Cu:C ratio under Fe limitation (Figure 1, Table 2 and S4), which is in agreement with the overexpression of plastocyanin and flavodoxin under reduced Fe availability. A previous study of metal contents in *Synechocystis sp.* under Fe limitation did not find a significant effect on

508 cellular Cu content; however, Fe limitation in that study was achieved through addition of a Fe-
509 chelating agent, deferoxamine B (Shcolnick et al. 2009), which may also bind to Cu (Farkas et
510 al. 1997) and limit its bioavailability. These contrasting effects of Fe limitation on Cu uptake by
511 *Synechocystis sp.* suggest that the method of lowering metal availability should be considered
512 in the experimental design of trace metal limitation studies.
513 The lower cellular Mn content in Fe-limited cells is in line with previous studies that
514 show Fe bioavailability affects Mn uptake (Shcolnick et al. 2009; Sharon et al. 2014). The Mn
515 concentration (9.2 μM) of normal composition BG-11 medium is sufficient for *Synechocystis sp.*
516 (Ogawa et al. 2002); thus Mn was not limiting under the growth conditions used in this study.
517 Mn, as a cofactor in the oxygen-evolving complex of PS II is required for oxygenic
518 photosynthesis (Shcolnick and Keren 2006) and the activity of PS II decreases under Fe
519 limitation in *Synechocystis sp.* (Ryan-Keogh et al. 2012; Sharon et al. 2014). Genes encoding
520 PSII components were strongly down-regulated in Fe-limited cultures (Kellom et al.,
521 unpublished).
522 Other trace metals showed a response to Fe limitation. Fe-limited cultures also had
523 lower chlorophyll a content (Figure 1, Table S4), suggesting thus a lower cellular demand for
524 Mg. Additionally, Mo is a key metal cofactor of enzymes involved in N assimilation (e.g., nitrate
525 reductase). Fe-limited *Synechocystis* showed significant reductions of Mo content and Mo:C
526 ration (Figure 1, Table S4) suggesting certain coordination between decreased Mo and N
527 uptake (Flores et al. 2005). This could be explained by the reduced Mo demand due the slower
528 growth under Fe limitation.
529
530 *Conclusions and potential implications in natural ecosystems*
531 The C:N:P stoichiometry and macromolecule composition of *Synechocystis sp.* changed
532 significantly under Fe limitation in ways that are consistent with the predictions of the GRH
533 (Elser et al. 1996) (Figure 2). This shows that limiting factors other than macronutrients, such

as Fe, may also induce lower growth rates through mechanisms involving changes in cellular N:P and Protein:RNA ratios. More work is needed to define the range of elemental and biological macromolecule compositions that *Synechocystis* produces under various conditions of nutrient availability and growth rates as this would permit insight into how growth responses of cyanobacteria in natural environments might alter the coupling of major biogeochemical cycles (C, N, P, Fe).

Our combined metabolomic, metallomic, stoichiometric, and macromolecular results show that Fe limitation responses of *Synechocystis* overlap with C and N limitation responses (Figure 2). Fe-limited *Synechocystis* also exhibited responses at the metabolomic level that indicate a state of oxidative stress and imbalance in the redox state of the cells. These insights aid in diagnosing the nutritional state of *Synechocystis sp.* in natural ecosystems. Microbial physiology underlies many biogeochemical processes and plays a crucial role in aquatic ecosystems (DeLong and Karl 2005). Enhancements of Fe limitation in natural aquatic ecosystems may result in significant impacts on their communities. Increases in the dissolution of $CO_2$ (Orr et al. 2005; Shi et al. 2012), nitric acid and/or ammonium (Vitousek et al. 1997; Bowman et al. 2008) in natural waters are potential drivers of acidification that could lead to significant reductions of Fe bioavailability for cyanobacteria (Shi et al. 2010; Shi et al. 2012). The understanding of metabolic changes of cyanobacteria under Fe limitation thus provide crucial insights into how those shifts in cells potentially scale to changes in ecosystem function by cascade effects through trophic webs (Figure 2).

**Acknowledgements**

The authors thank Laia Mateu-Castell, Laura Steger, Zarraz Lee, Jessica Corman, Krist Rouypirom, Zureyma Martinez, Matthew Kellom, Wei Deng, and Jennifer Learned for their laboratory support. Thanks to Ravi Vannela for providing *Synechocystis sp*. PCC 6803 and Wim Vermaas for helpful discussion of the data. ARU appreciates the financial support of the

research fellowship (JAE) from the CSIC. This research was supported by the Spanish Government Project CGL2013-48074-P and the Catalan Government Project SGR 2014-274, the European Research Council (Synergy Grant SyG-2013-610028, IMBALANCE-P), and the NASA Astrobiology Institute at Arizona State University (Follow the Elements; NAI5-0018). A portion of the research was performed using EMSL, a DOE Office of Science User Facility sponsored by the Office of Biological and Environmental Research at the Pacific Northwest National Laboratory. MO and OU were supported by the Ministry of Education, Youth and Sports within grants LO1415 and LM2015061.ATPP and JJE were supported by the ASU NASA Astrobiology Institute.

**Author contributions:** AR-U and AP-P performed the research and performed the statistical analyses. AR-U and AP-P wrote the manuscript. AR-U, AP-P, JE, JP and JS designed the research. AP-P performed the elemental analyses. MO, OU, MP-T, CL-Q performed the metabolomic analyses with LC-MS and NMR. JP, JS and JE funded the research. All authors have read, commented and approved the final version of the manuscript.

586 **References**

587

588 Allen MM (1968) Simple conditions for growth of unicellular blue-green algae on plates. J
589 Phycol 4:1–4.
590 Baniulis D., Yamashita E., Zhang H., Hasan SS., Cramer WA (2008) Structure-Function of the
591 cytochrome $b_6f$ complex. Photochem Photobiol 84:1349-1358.
592 Behrenfeld M., Bale A., Kolber Z., et al (1996) Confirmation of Iron Limitation of Phytoplankton
593 Photosynthesis in the Equatorial Pacific-Ocean. Nature 383:508–511.
594 Behrenfeld MJ (1999) Widespread Iron Limitation of Phytoplankton in the South Pacific Ocean.
595 Science (80- ) 283:840–843.
596 Behrenfeld MJ, Milligan AJ (2013) Photophysiological expressions of iron stress in
597 phytoplankton. Ann Rev Mar Sci 5:217–46.
598 Bellenger J-P, Wichard T, Xu Y, Kraepiel AML (2011) Essential metals for nitrogen fixation in a
599 free-living $N_2$-fixing bacterium: chelation, homeostasis and high use efficiency. Environ
600 Microbiol 13:1395–411.
601 Bennette NB, Eng JF, Dismukes GC (2011) An LC-MS-based chemical and analytical method for
602 targeted metabolite quantification in the model cyanobacterium Synechococcus sp. PCC
603 7002. Anal Chem 83:3808–16.
604 Bibby TS, Nield J, Barber J (2001) Iron deficiency induces the formation of an antenna ring
605 around trimeric photosystem I in cyanobacteria. Nature 412:743–745.
606 Bowman WD, Cleveland CC, Halada Ĺ, et al (2008) Negative impact of nitrogen deposition on
607 soil buffering capacity. Nat Geosci 1:767–770.
608 Castielli O, De la Cerda B, Navarro JA, et al (2009) Proteomic analyses of the response of
609 cyanobacteria to different stress conditions. FEBS Lett 583:1753–8.
610 Cooley JW, Vermaas WF (2001) Succinate dehydrogenase and other respiratory pathways in
611 thylakoid membranes of Synechocystis sp. strain PCC 6803: capacity comparisons and

physiological function. J Bacteriol 183:4251–8.

Dang TC, Fujii M, Rose AL, et al (2012) Characteristics of the freshwater cyanobacterium Microcystis aeruginosa grown in iron-limited continuous culture. Appl Environ Microbiol 78:1574–83.

Dejean S, Gonzalez I, Le Cao K (2013) mixOmics: Omics Data Integration Project.

DeLong EF, Karl DM (2005) Genomic perspectives in microbial oceanography. Nature 437:336–42.

Elser JJ, Dobberfuhl DR, MacKay NA, Schampel JH (1996) Organism Size, Life History, and N:P Stoichiometry. Bioscience 46:674–684.

Elser JJ, Sterner RW, Gorokhova E, et al (2008) Biological stoichiometry from genes to ecosystems. Ecol Lett 3:540–550.

Farkas E, Csóka H, Micera G, Dessi A (1997) Copper(II), nickel(II), zinc(II), and molybdenum(VI) complexes of desferrioxamine B in aqueous solution. J Inorg Biochem 65:281–286.

Ferreira F, Straus NA (1994) Iron deprivation in cyanobacteria. J Appl Phycol 6:199–210.

Fiehn O (2002) Metabolomics - the link between genotypes and phenotypes. Plant Mol Biol 48:155–171.

Flores E, Frías JE, Rubio LM, Herrero A (2005) Photosynthetic nitrate assimilation in cyanobacteria. Photosynth Res 83:117–33.

Fox J, Weisberg S (2011) An {R} Companion to Applied Regression. R package.

Gargallo-Garriga A, Sardans J, Pérez-Trujillo M, et al (2014) Opposite metabolic responses of shoots and roots to drought. Sci Rep 4:6829.

Gargallo-Garriga A, Sardans J, Pérez-Trujillo M, et al (2015) Warming differentially influences the effects of drought on stoichiometry and metabolomics in shoots and roots. New Phytol 207:591–603.

Gründel M, Scheunemann R, Lockau W, Zilliges Y (2012) Impaired glycogen synthesis causes metabolic overflow reactions and affects stress responses in the cyanobacterium

638 Synechocystis sp. PCC 6803. Microbiology 158:3032–43.
639 Hagemann M (2011) Molecular biology of cyanobacterial salt acclimation. FEMS Microbiol Rev
640 35:87–123.
641 Hasunuma T, Kikuyama F, Matsuda M, et al (2013) Dynamic metabolic profiling of
642 cyanobacterial glycogen biosynthesis under conditions of nitrate depletion. J Exp Bot
643 64:2943–54.
644 Hernández-Prieto MA, Schön V, Georg J, et al (2012) Iron deprivation in Synechocystis:
645 inference of pathways, non-coding RNAs, and regulatory elements from comprehensive
646 expression profiling. G3 (Bethesda) 2:1475–95.
647 Houshyani B, Kabouw P, Muth D, et al (2012) Characterization of the natural variation in
648 Arabidopsis thaliana metabolome by the analysis of metabolic distance. Metabolomics
649 8:131–145.
650 Huege J, Goetze J, Schwarz D, et al (2011) Modulation of the major paths of carbon in
651 photorespiratory mutants of synechocystis. PLoS One 6:e16278.
652 Jones OAH, Maguire ML, Griffin JL, et al (2013) Metabolomics and its use in ecology. Austral
653 Ecol 38:713–720.
654 Kaneko T, Sato S, Kotani H, et al (1996) Sequence Analysis of the Genome of the Unicellular
655 Cyanobacterium Synechocystis sp. Strain PCC6803. II. Sequence Determination of the
656 Entire Genome and Assignment of Potential Protein-coding Regions. DNA Res 3:109–
657 136.
658 Katoh H, Hagino N, Grossman AR, Ogawa T (2001a) Genes essential to iron transport in the
659 cyanobacterium Synechocystis sp. strain PCC 6803. J Bacteriol 183:2779–84.
660 Katoh H, Hagino N, Ogawa T (2001b) Iron-binding activity of FutA1 subunit of an ABC-type iron
661 transporter in the cyanobacterium Synechocystis sp. Strain PCC 6803. Plant Cell Physiol
662 42:823–7.
663 Keren N, Aurora R, Pakrasi HB (2004) Critical roles of bacterioferritins in iron storage and

664 proliferation of cyanobacteria. Plant Physiol 135:1666–73.
665 Knoop H, Gründel M, Zilliges Y, et al (2013) Flux balance analysis of cyanobacterial metabolism:
666 the metabolic network of Synechocystis sp. PCC 6803. PLoS Comput Biol 9:e1003081.
667 Kopf M, Klähn S, Scholz I, et al (2014) Comparative analysis of the primary transcriptome of
668 Synechocystis sp. PCC 6803. DNA Res 21:527–39.
669 Kranzler C, Lis H, Finkel OM, et al (2014) Coordinated transporter activity shapes high-affinity
670 iron acquisition in cyanobacteria. ISME J 8:409–17.
671 Krieg N., Parte A, Ludwig W, et al (2010) Bergey's Manual of Systematic Bacteriology: Volume
672 4: The Bacteroidetes, Spirochaetes, Tenericutes (Mollicutes), Acidobacteria,
673 Fibrobacteres, Fusobacteria, Dictyoglomi, Gemmatimonadetes, Lentisphaerae,
674 Verrucomicrobia, Chlamydiae, and Planctomycetes. Springer New York, New York, NY
675 Latifi A, Ruiz M, Zhang C-C (2009) Oxidative stress in cyanobacteria. FEMS Microbiol Rev
676 33:258–78.
677 Lee DY, Fiehn O (2013) Metabolomic response of Chlamydomonas reinhardtii to the inhibition
678 of target of rapamycin (TOR) by rapamycin. J Microbiol Biotechnol 23:923–31.
679 Leiss KA, Cristofori G, van Steenis R, et al (2013) An eco-metabolomic study of host plant
680 resistance to Western flower thrips in cultivated, biofortified and wild carrots.
681 Phytochemistry 93:63–70.
682 Lengeler J, Drews G, Schlegel H. (1999) Biology of the Prokaryotes. Hoboken, NJ: Wiley-
683 Blackwell, pp. 1-984 .
684 Macel M, Van Dam NM, Keurentjes JJB (2010) Metabolomics: the chemistry between ecology
685 and genetics. Mol Ecol Resour 10:583–93.
686 Mackey KRM, Post AF, McIlvin MR, et al (2015) Divergent responses of Atlantic coastal and
687 oceanic Synechococcus to iron limitation. Proc Natl Acad Sci U S A 112:9944–9949.
688 Maeda H, Sakuragi Y, Bryant DA, Dellapenna D (2005) Tocopherols protect Synechocystis sp.
689 strain PCC 6803 from lipid peroxidation. Plant Physiol 138:1422–35.

690 Mari A, Lyon D, Fragner L, et al (2013) Phytochemical composition of Potentilla anserina L.
691 analyzed by an integrative GC-MS and LC-MS metabolomics platform. Metabolomics
692 9:599–607.
693 Ogawa T, Bao DH, Katoh H, et al (2002) A two-component signal transduction pathway
694 regulates manganese homeostasis in Synechocystis 6803, a photosynthetic organism. J
695 Biol Chem 277:28981–6.
696 Oksanen J, Guillaume-Blanchet F, Kindt R, et al (2013) vegan: Community Ecology Package.
697 Orr JC, Fabry VJ, Aumont O, et al (2005) Anthropogenic ocean acidification over the twenty-
698 first century and its impact on calcifying organisms. Nature 437:681–6.
699 Osanai T, Oikawa A, Shirai T, et al (2014) Capillary electrophoresis-mass spectrometry reveals
700 the distribution of carbon metabolites during nitrogen starvation in Synechocystis sp. PCC
701 6803. Environ Microbiol 16:512–24.
702 Papageorgiou GC, Murata N (1995) The unusually strong stabilizing effects of glycine betaine
703 on the structure and function of the oxygen-evolving Photosystem II complex.
704 Photosynth Res 44:243–52.
705 Peñuelas J, Sardans J (2009) Ecological metabolomics. Chem Ecol 25:305–309.
706 Pluskal T, Castillo S, Villar-Briones A, Orešič M (2010) MZmine 2: modular framework for
707 processing, visualizing, and analyzing mass spectrometry-based molecular profile data.
708 BMC Bioinformatics 11:395.
709 R Core Team (2013) R: A language and environment for statistical computing. R package.
710 Raven JA, Evans MCW, Korb RE (1999) The role of trace metals in photosynthetic electron
711 transport in O2-evolving organisms. Photosynth Res 60:111–150.
712 Richardson DJ (2000) Bacterial respiration: a flexible process for a changing environment.
713 Microbiology 146 Pt 3:551–71.
714 Rivas-Ubach A, Gargallo-Garriga A, Sardans J, et al (2014) Drought enhances folivory by shifting
715 foliar metabolomes in Quercus ilex trees. New Phytol 202:874–885.

716 Rivas-Ubach A, Pérez-Trujillo M, Sardans J, et al (2013) Ecometabolomics: optimized NMR-
717 based method. Methods Ecol Evol 4:464–473.
718 Rivas-Ubach A, Barbeta A, Sardans J, et al (2016a) Topsoil depth substantially influences the
719 responses to drought of the foliar metabolomes of Mediterranean forests. Perspect Plant
720 Ecol Evol Syst 21:41–54.
721 Rivas-Ubach A, Sardans J, Hódar JA, et al (2016b) Similar local but different systemic
722 metabolomic responses of closely related pine subspecies to folivory by caterpillars of the
723 processionary moth. Plant Biol 18:484–494.
724 Rivas-Ubach A, Hódar JA, Sardans J, et al (2016c) Are the metabolic responses to folivory of
725 colsely related plant species linked to macroevolutionary and plant-folivore
726 coevolutionary processes? Ecol Evol 6: 4372-4386.
727 Rivas-Ubach A, Sardans J, Hódar JA, et al (2017) Close and distant: Contrasting the metabolism
728 of two closely related subspecies of Scots pine under the effects of folivory and summer
729 drought. Ecol Evol DOI: 10.1002/ece3.3343.
730 Rivas-Ubach A, Sardans J, Pérez-Trujillo M, et al (2012) Strong relationship between elemental
731 stoichiometry and metabolome in plants. Proc Natl Acad Sci 109:4181–4186.
732 Ryan-Keogh TJ, Macey AI, Cockshutt AM, et al (2012) The cyanobacterial chlorophyll-binding-
733 protein IsiA acts to increase the in vivo effective absorption cross-section of psi under
734 iron limitation. J Phycol 48:145–154.
735 Ryan-Keogh TJ, Macey AI, Cockshutt AM, et al (2012) The cyanobacterial chlorophyll-binding-
736 protein isia acts to increase the in vivo effective absorption cross-section of psi under iron
737 limitation. J Phycol 48:145–154.
738 Sharon S, Salomon E, Kranzler C, et al (2014) The hierarchy of transition metal homeostasis:
739 iron controls manganese accumulation in a unicellular cyanobacterium. Biochim Biophys
740 Acta 1837:1990–7.
741 Shcolnick S, Keren N (2006) Metal homeostasis in cyanobacteria and chloroplasts. Balancing

742 benefits and risks to the photosynthetic apparatus. Plant Physiol 141:805–10.
743 Shcolnick S, Summerfield TC, Reytman L, et al (2009) The mechanism of iron homeostasis in
744 the unicellular cyanobacterium synechocystis sp. PCC 6803 and its relationship to
745 oxidative stress. Plant Physiol 150:2045–56.
746 Shi D, Kranz SA, Kim J-M, Morel FMM (2012) Ocean acidification slows nitrogen fixation and
747 growth in the dominant diazotroph Trichodesmium under low-iron conditions. Proc Natl
748 Acad Sci U S A 109:E3094-100.
749 Shi D, Xu Y, Hopkinson BM, Morel FMM (2010) Effect of ocean acidification on iron availability
750 to marine phytoplankton. Science 327:676–9.
751 Silva JJRF da, Williams RJP (2001) The Biological Chemistry of the Elements: The Inorganic
752 Chemistry of Life. Oxford University Press, New York. pp. 1-583. ISBN: 0198508484.
753 Singh AK, Chakravarthy D, Singh TPK, Singh HN (1996) Evidence for a role for L-proline as a
754 salinity protectant in the cyanobacterium Nostoc muscorum. Plant, Cell Environ 19:490–
755 494.
756 Singh AK, Li H, Sherman LA (2004) Microarray analysis and redox control of gene expression in
757 the cyanobacterium Synechocystis sp. PCC 6803. Physiol Plant 120:27–35.
758 Sterner R, Elser J (2002) Ecological Stoichiometry: The Biology of Elements from Molecules to
759 the Biosphere. Princetion University Press, Princenton. pp. 1-439. ISBN: 0691074909
760 Steuer R, Kurths J, Fiehn O, Weckwerth W (2003) Observing and interpreting correlations in
761 metabolomic networks. Bioinformatics 19:1019–1026.
762 Sumner LW, Amberg A, Barrett D, et al (2007) Proposed minimum reporting standards for
763 chemical analysis. Metabolomics 3:211–221.
764 Szabados L, Savouré A (2010) Proline: a multifunctional amino acid. Trends Plant Sci 15:89–97.
765 t'Kindt R, De Veylder L, Storme M, et al (2008) LC-MS metabolic profiling of Arabidopsis
766 thaliana plant leaves and cell cultures: optimization of pre-LC-MS procedure parameters.
767 J Chromatogr B Analyt Technol Biomed Life Sci 871:37–43.

768 Tovar-Sanchez A, Sañudo-Wilhelmy SA, Garcia-Vargas M, et al (2003) A trace metal clean
769 reagent to remove surface-bound iron from marine phytoplankton. Mar Chem 82:91–99.
770 Vitousek PM, Aber JD, Howarth RW, et al (1997) Human alteration of the global nitrogen cycle:
771 sources and cosequences. Ecol Appl 7:737–750.
772 Vrede T, Tranvik LJ (2006) Iron Constraints on Planktonic Primary Production in Oligotrophic
773 Lakes. Ecosystems 9:1094–1105.
774 Wilson A, Boulay C, Wilde A, et al (2007) Light-Induced Energy Dissipation in Iron-Starved
775 Cyanobacteria: Roles of OCP and IsiA Proteins.
776 Yoshikawa K, Hirasawa T, Ogawa K, et al (2013) Integrated transcriptomic and metabolomic
777 analysis of the central metabolism of Synechocystis sp. PCC 6803 under different
778 trophic conditions. Biotechnol J 8:571–80.
779
780
781
782
783
784
785
786
787
788
789
790
791
792
793
794
795
796
797

798 **Table 1**. PERMANOVA results table obtained from the metabolomic dataset including the
799 identified and non-identified data with treatment as fixed independent factor.

| | Degrees of freedom | Sum of Squares | Mean Square | Pseudo-F | *P* |
|---|---|---|---|---|---|
| Treatment | 1 | $2.7\times10^{18}$ | $2.7\times10^{18}$ | 15.4 | 0.0023 |
| Residuals | 10 | $1.7\times10^{18}$ | $1.7\times10^{17}$ | | |
| Total | 11 | $4.4\times10^{18}$ | | | |

800
801
802
803
804
805
806
807
808
809
810
811
812
813
814
815
816
817
818
819

820 **Table 2**. Metal-to-C ratios of *Synechocystis sp*. PCC 6803 grown in complete (N:P 100, Fe 18
821 μM) and Fe-limited (N:P 100, Fe 1.8 μM) BG-11 media. Values listed are the average ± S.D.

822 (n=6). Statistical differences between complete and Fe-limited cultures were assessed using a
823 two-sided t-test or a Mann-Whitney U test.

| Me:C | Complete | Fe-limited | df | t | U | *P* |
|---|---|---|---|---|---|---|
| mmol mol$^{-1}$ | | | | | | |
| $^{56}$Fe | 0.28 ± 0.08 | 0.10 ± 0.01 | 5.89 | 6.89 | | <0.001 |
| $^{44}$Ca | 80.35 ± 28.28 | 104.93 ± 9.84 | 6.19 | -2.01 | | n.s. |
| $^{24}$Mg | 4.33 ± 0.59 | 3.21 ± 0.13 | 5.81 | 4.86 | | 0.003 |
| µmol mol$^{-1}$ | | | | | | |
| $^{55}$Mn | 15.20 ± 9.21 | 2.63 ± 0.38 | | | 36 | 0.002 |
| $^{66}$Zn | 11.73 ± 6.02 | 9.17 ± 0.98 | | | 19 | n.s. |
| $^{63}$Cu | 1.19 ± 0.25 | 1.98 ± 0.13 | 7.67 | -6.92 | | <0.001 |
| $^{60}$Ni | 1.17 ± 0.26 | 1.29 ± 0.17 | 8.52 | -0.92 | | n.s. |
| $^{59}$Co | 0.73 ± 0.21 | 0.62 ± 0.04 | | | 21 | n.s. |
| $^{51}$V | 0.032 ± 0.015 | 0.019 ± 0.003 | | | 28 | n.s. |
| nmol mol$^{-1}$ | | | | | | |
| $^{95}$Mo | 57.61 ± 19.51 | 38.72 ± 5.33 | | | 31 | 0.041 |

824
825
826
827
828
829
830
831
832
833
834

835 **Figure 1.** Principal component 1 (PC1) of the principal component analysis (PCA) of the
836 elemental, stoichiometric, macromolecular and metabolomic variables in *Synechocystis sp.* PCC
837 6803. Panel **a** shows the PC1 of the variables plot of complete versus Fe-limited cultures. Bars
838 represent the loadings along the PC1 for each of the variables and have been represented in
839 different colors. Growth rate (GR) and cell density are shown in orange. C, N, P, S, and C:N:P
840 ratios are shown in red. Chlorophyll a, DNA, RNA, Protein, and their ratios are shown in violet.

Metals (Fe, Ca, Mg, Mn, Zn, Cu, Ni, Co, Mo and V) are shown in grey. Different metabolite classes are also represented in different colors: blue: carbohydrates; cyan: nucleotides; green: amino acids; yellow: organic acids and brown: other secondary metabolites. Abbreviations have been used for several metabolites: adenosine monophosphate (AMP), uridine monophosphate (UMP), thymidine monophosphate (TMP), Nicotinamide adenine dinucleotide (NAD+), alanine (Ala), arginine (Arg), methionine (Met), phenylalanine (Phe), leucine (Leu), proline (Pro), serine (Ser), threonine (Thr), tryptophan (Trp), tyrosine (Tyr), valine (Val), lysine (Lys), NMR overlapping signal of lysine and alanine (Lys.Ala), glutamine (Gln), glutamate (Glu), aspartic acid (Asp.ac), citric acid (Citric.ac), lactic acid (Lactic.ac), malic acid (Malic.ac), pyruvic acid (Pyruvic.ac) and, succinic acid (Succinic.ac). Panel **b** shows the PC1 of the cases plot categorized by treatment (blue: complete cultures; red: Fe-limited cultures). Variables marked with asterisks showed statistical significance ($P < 0.05$) and variables marked with crosses showed marginal statistical significance ($P < 0.1$) in t-tests (Tables S4 and S5 of Supporting Information).

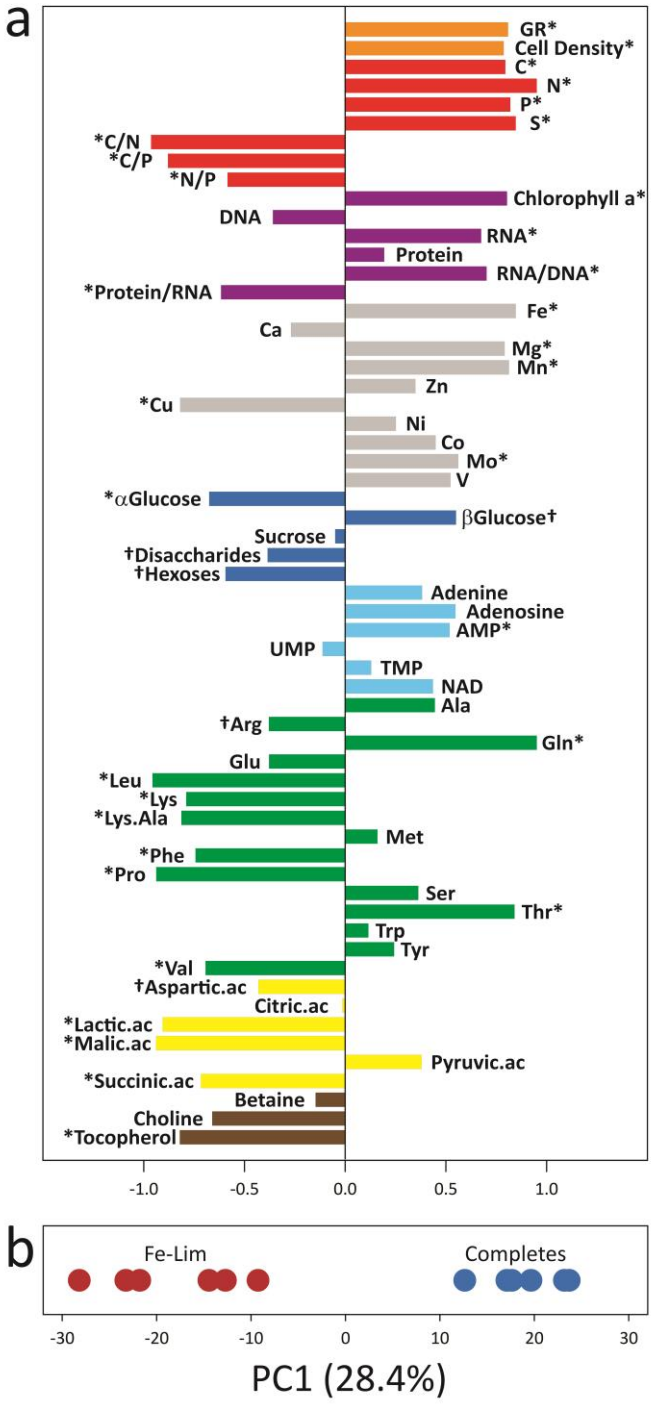
a
GR*
Cell Density*
C*
N*
P*
S*
*C/N
*C/P
*N/P
Chlorophyll a*
DNA
RNA*
Protein
RNA/DNA*
*Protein/RNA
Fe*
Ca
Mg*
Mn*
Zn
*Cu
Ni
Co
Mo*
V
*αGlucose
βGlucose†
Sucrose
†Disaccharides
†Hexoses
Adenine
Adenosine
AMP*
UMP
TMP
NAD
Ala
†Arg
Gln*
Glu
*Leu
*Lys
*Lys.Ala
Met
*Phe
*Pro
Ser
Thr*
Trp
Tyr
*Val
†Aspartic.ac
Citric.ac
*Lactic.ac
*Malic.ac
Pyruvic.ac
*Succinic.ac
Betaine
Choline
*Tocopherol
-1.0
-0.5
0.0
0.5
1.0
b
Fe-Lim
Completes
-30
-20
-10
0
10
20
30
PC1 (28.4%)

861

**Figure 2.** Summary of the main metabolomic, macromolecular, elemental and stoichiometric responses of *Synechocystis sp.* PCC 6803 to iron limitation which consequently lead to lower growth rates.